Vortex dynamics and phase diagram of BSCCO in the presence of columnar defects

2000 J. Phys.: Condens. Matter 12 4217

(http://iopscience.iop.org/0953-8984/12/18/307)

J. Phys.: Condens. Matter **12** (2000) 4217–4231. Printed in the UK PII: S0953-8984(00)09053-6

Vortex dynamics and phase diagram of BSCCO in the presence of columnar defects

L Ammor†, R De Sousa†, J C Soret†, V Ta Phuoc†, A Ruyter†, A Wahl‡ and E Olive†

† Laboratoire d'Electrodynamique des Matériaux Avencés§, Université F Rabelais, UFR Sciences, Parc de Grandmont, 37200 Tours, France

‡ Laboratoire CRIMAT, ISMRA et Université de Caen, UMR 6508, associée au CNRS, 6 Boulevard Marechal Juin, 14050 Caen Cedex, France

Received 28 October 1999, in final form 9 March 2000

E-mail: ammor@delphi.phys.univ-tours.fr

Abstract. Current–voltage characteristics are investigated in $BiSr_2CaCu_2O_8$ single crystals irradiated parallel to the c-axis with 5.8 GeV Pb ions. For weak magnetic field ($B < B_\Phi$), we find that isothermal I–V curves scale according to the Bose-glass (BG) theory. Field and sample independent critical exponent $z' = 5.27 \pm 0.05$ and $\nu' = 1.30 \pm 0.07$ have been found. The magnetic field dependence of the BG melting line $T_{BG}(B)$, derived from critical scaling analysis, is in good agreement with the Lindemann criterion which accounts for the contribution of correlated disorder. Two characteristic temperatures $T_0 \approx 0.72\ T_c$ ($f \approx 0.8$) and $T_1 \approx 0.83\ T_c$ ($f \approx 1/3$), beyond which the vortex system is increasingly dominated by vortex–vortex interactions (high field) or thermal fluctuations (high temperature), are identified. We obtain good quantitative agreement between our experimental data and the predictions of the Bose-glass theory for correlated disorder.

1. Introduction

The structure of the different possible vortex states in the B–T phase diagram and the nature of the thermodynamic transitions between the phases have become central issues for the physics of the mixed state of high-temperature superconductors [1]. Combined effects of thermal fluctuations, electronic anisotropy, dimensionality and disorder lead to a rich magnetic phase diagram. It is now generally admitted that a phase transition separates a high temperature vortex-liquid-like state from a low-temperature phase, consisting of a vortex lattice or Bragg glass [2] with a long-range positional order, undergoing a first-order melting transition due to enhanced thermal fluctuations. In the presence of a strong pinning, the vortex liquid phase freezes via a second-order transition into a vortex glass. The nature of both the freezing transition and the vortex glass depends essentially on the defects' dimensionality, i.e. point (0D), correlated (1D or 2D) disorder [3–5]. In the case of columnar defects produced by heavy-ion irradiation (correlated disorder), according to the analogy between the vortex system and the physics of 2D bosons, at low temperatures and below the matching field B_Φ (where the vortex density equals the defect density), a Bose-glass (BG) phase has been predicted by Nelson and Vinokur (NV) [4], with strong localization of vortices lines on columnar defects (CDs).

§ Unité propre de recherche de l'Enseignement Supérieur associée au CNRS et Laboratoire de Recherche Correspondant du CEA.

0953-8984/00/184217+15$30.00

At higher temperatures the BG phase melts into an entangled vortex liquid through a second-order transition at $T_{BG}(B)$. It has been clearly demonstrated in many experimental studies that, for fields below the matching field B_Φ, the resulting $T_{BG}(B)$ line separating vortex liquid and solid states is shifted to higher temperatures from the melting line $T_m(B)$ of an unirradiated sample [6–9]. Nevertheless, the magnetic phase diagram, in particular the behaviour of Bose-glass line $T_{BG}(B)$ and its comparison with theoretical predictions in different fields regions, is still a widely discussed topic in high-T_c oxide superconductors. Experimentally, this subject is even more complex. Indeed, it was generally shown that the extracted BG line might be affected by sample-dependent properties such as the density of tracks, material anisotropy or by experimental techniques which are used to identify the BG melting temperature T_{BG} (peak of the ac magnetic susceptibility χ'', onset of the third harmonic in the ac susceptibility response, disappearance of the ohmic behaviour etc). For example, the anisotropy effect should be noticed in experimental investigations conducted on three-dimensional $YBa_2Cu_3O_{7-\delta}$ (YBCO) superconductor crystals and on a nearly two-dimensional superconductor like $Bi_2Sr_2CaCu_2O_8$ (BSCCO). Indeed, for the same CD densities, the Bose-glass line $T_{BG}(B)$ behaviours between YBCO and BSCCO differ [10, 11].

The effect of the strong pinning, in particular the pinning due to linear defects introduced by heavy ion irradiation, on the position of the melting line in the B–T phase diagram has been studied theoretically in different field regimes [1, 4, 12]. Theoretical predictions, in the case of moderate fields $B < B_\Phi$ (i.e. columnar defects outnumber the vortex lines), have been successfully applied to describe the phase diagram when $B/B_\Phi \leqslant 0.5$ in the irradiated Y-123 single crystals with several irradiation doses [8, 13, 14]. However, experimental data show that in the case of highly anisotropic material such as BSCCO the phase diagram is more complicated. In BSCCO single crystals irradiated with a dose equivalent to $B_\Phi = 200$ mT at 45°to the c-axis [6], the situation seems to be very different. Indeed, the form of the $T_{BG}(B)$ line extracted from magnetic measurements performed with the field B parallel to the defects cannot be analysed in terms of a simple shift of the vortex lattice melting transition but follows at low field the crossover line $B^*(T)$ introduced in [1, 4], separating in the Bose-glass phase the single-vortex regime from the bundle regime, and approaches the virgin material melting line at high fields. Nevertheless, the Bose-glass line in the latter case is also described using equation (4) (see below) but only for temperatures above the depinning temperature $T > T_1$ (i.e. higher temperature regime). Other experiments, have also revealed that the introduction of CDs in BSCCO crystals changes the interlayer Josephson coupling in the vortex fluid phase above the transition line, in particular, the recoupling of decoupled vortex lines at a critical field of $B/B_\Phi \approx 1/3$ [15, 16].

Above the matching field $B \geqslant B_\Phi$, the behaviour becomes more complicated as vortices now outnumber the columnar defects. However, as pointed out by Radzihovsky *et al* [17] and Wengel and Tauber [18], a reported BG phase diagram can discriminate between two regimes of strongly ($B < B_\Phi$) and weakly ($B \geqslant B_\Phi$) pinned Bose-glass (SBG and WBG, respectively) phase separated in the B–T plane by the interaction field $B^*(T)$. In the latter regime, an arrangement of flux lines bound to defects forms a cage for other vortices and pins them through their mutual interactions.

The present paper reports on the vortex phase diagram in Y and Pb substituted BSCCO single crystals in the presence of columnar defects parallel to the c-axis, using transport measurements. We have examined the behaviour of the isothermal current–voltage characteristics for magnetic fields parallel to the c-axis. Over a wide range of filling factor $0.026 \leqslant f = B/B_\Phi \leqslant 1$, I–V curves near the superconducting transition are consistent with the Bose-glass scaling theory. Field and sample independent critical exponent values $z' = 5.27 \pm 0.05$ and $\nu' = 1.3 \pm 0.07$ have been found. The magnetic field dependence of

the BG transition temperature $T_{BG}(B)$ in various regimes has been extracted from the scaling analysis. For magnetic field range $0.3\ B_\Phi < B < B_\Phi$, using typical material parameters for BSCCO, we find that the Bose-glass line $T_{BG}(B)$ is well described by the Lindemann criterion which accounts for the contribution of columnar defects (equation (4)). However, beyond this regime, where the vortex–vortex interactions or thermal fluctuations begin to dominate the correlated disorder pinning effect, the $T_{BG}(B)$ of irradiated crystals merges the pristine line determined from low resistivity criterion, as predicted by theoretical and experimental reports [1, 4, 6].

2. Experimental procedures

Vortex dynamics are studied in $Bi_2Sr_2CaCu_2O_8$ single crystals, which have different physical properties before the irradiation. It has previously been established that the pinning properties of Bi-2212 are very sensitive to doping level, which can be modified by Y and Pb substitution on the Ca and Bi site, respectively [19, 20]. Thus, for example the substitution of Y^{3+} for Ca^{2+} in $Bi_2Sr_2Ca_{1-x}Y_xCu_2O_{8+\delta}$ varies the doping level of the CuO_2 planes from the overdoped to the underdoped regime with an optimum level of T_c at $x \approx 0.28$. In return, the Pb substitution in $Bi_{2-y}Pb_ySr_2CaCu_2O_{8+\delta}$ single crystals results in an increase in the carrier concentration, which may lead to the overdoped region of the phase diagram in comparison with the Pb-free samples [21]. Three Bi-2212 single crystals were used in this study: Bi[Pb]-2212 (sample 1), Bi-2212 (sample 2) and Bi[Y]-2212 (sample 3). All of them were grown by the same self-flux method which has been described elsewhere [22, 23]. These samples are overdoped for Bi 2212 and Bi[Pb]-2212 (with $y = 0.20$) and underdoped for Bi[Y]-2212 (with $x = 0.36$). The samples with typical dimensions of $1 \times 1 \times 0.3$ mm^3 have been irradiated with 5.8 GeV Pb ions at Ganil (Caen, France). Columnar ion tracks of diameter $2C_0 \approx 70$–90 Å were created along the c-axis [24]. The samples were irradiated with a dose of 3.75×10^{10} Pb cm^{-2} for sample 1, 7.5×10^{10} Pb cm^{-2} for sample 2 and 3.75×10^{10} Pb cm^{-2} for sample 3. These fluences expressed in term of matching field B_Φ ($B_\Phi = \Phi_0/d^2$ where Φ_0 is the elementary flux quantum and d is the mean distance between defects) were 0.75 T for sample 1 and 3 and 1.5 T for sample 2. Isothermal I–V characteristics were obtained by using a d.c. four-probe method with a voltage resolution of 10^{-10} V and a temperature stability better than 5 mK. Currents up to 100 mA were used without heating effects detected from the temperature controller. For all samples, the zero field ohmic resistance as a function of the temperature did not exhibit any shoulder or other anomaly, and an estimate of the width of the superconducting transition ΔT is obtained from the width measured at half-maximum, of the single $\mathrm{d}R/\mathrm{d}T$. In this way, the transition temperatures were found to be $T_c = 80.0$, 89.5 and 91.2 K and the transition widths $\Delta T = 1.0$–1.5 K for samples 1, 2 and 3, respectively.

3. Results and discussion

The angular dependence of the resistivity is systematically investigated on all irradiated samples. Figure 1 shows an example of the resistance, as a function of the angle, θ, between the c-axis and the applied field, taken at $T = 70.86$ K. For the lowest T and $B < B_\Phi$ values, the $R(\theta)$ curves exhibit a clear dip occurring at $\theta = 0$ i.e. when the field is applied along the columnar ion tracks. This feature is a manifestation of 3D vortex line behaviour since such a directional effect cannot be expected for independent 2D pancake vortices (figure 1(a)). The magnetic field was aligned with the columnar defects using the dip occurring in dissipation for fields parallel the CDs at filling factors $f = B/B_\Phi < 1$.

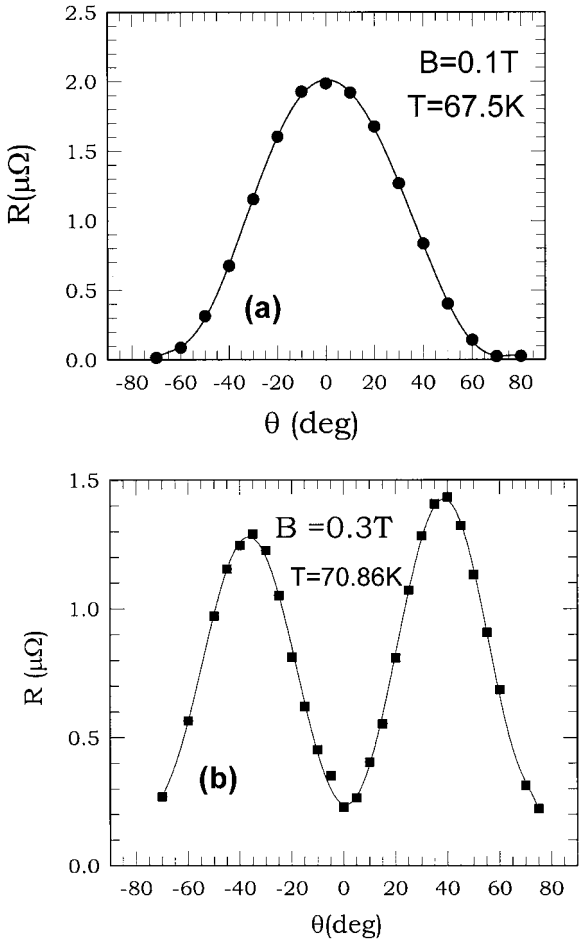

Figure 1. The typical angular dependence of the resistance, as a function of the angle, θ, between the c-axis and the applied magnetic field: (a) unirradiated sample and (b) after irradiation.

3.1. Universal Bose-glass scaling

We have examined the behaviour of I–V curves, near the glass–liquid transition at a well defined temperature from a resistive state into a superconducting state ($R \equiv V/I = 0$, in the low current density limit) upon cooling, in applied magnetic field B less than B_Φ along the c-axis, i.e. the flux lines parallel to the CDs. Figure 2 displays a typical log–log plot of the I–V curves obtained for $B = 0.85$ T for sample 2. One can notice a nonlinear behaviour of the curves at lower temperatures whereas the upper curves exhibit a linear regime in the limit of low currents. As shown in figure 2, the transition from ohmic to non-ohmic behaviour occurs around $T = T_{BG}$, with decreasing T. Such behaviour is consistent with the BG transition theory [1, 4]. According to the predictions for the BG transition in the presence of columnar defects, scaling laws based on a second-order phase transition hold for the regions above and below the BG transition temperature. In this approach, the electric field E and current density J are related by

$$(E/J) = (\ell_\parallel/\ell_\perp^{z'})F_\pm(x) \qquad x = J\ell_\parallel\ell_\perp\Phi_0/K_BT \tag{1}$$

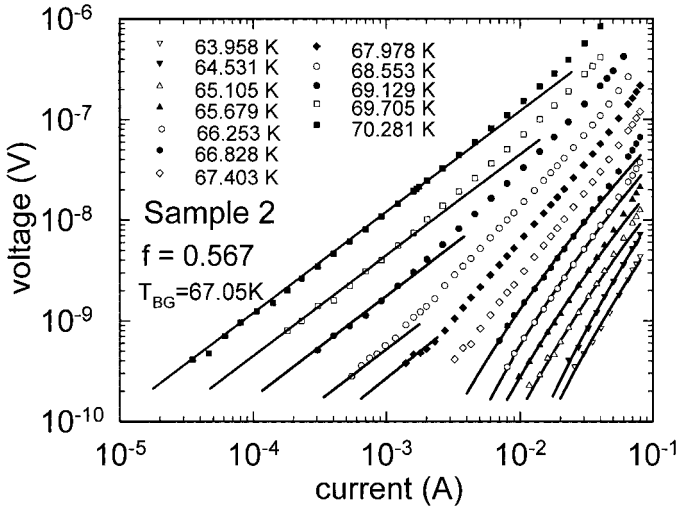

Figure 2. Logarithmic plot of isothermal I–V curves for B fixed. The straight lines display a fit of the ohm law. The curved lines are a fit according to equation (2) (with $\mu = 1/3$) to the data obtained for weak currents.

where E is the electric field, J is the current density and F_+ and F_- are scaling functions defined in the flux liquid state ($T > T_{BG}$) and localized flux-line state ($T < T_{BG}$), respectively. The anisotropy of pinning properties due to the uniaxial nature of the defects leads to $\ell_\perp(T) = \ell_\perp(0)|(T - T_{BG})/T_{BG}|^{-\nu_\perp}$ and $\ell_\parallel(T) = \ell_\parallel(0)|(T - T_{BG})/T_{BG}|^{-\nu_\parallel}$, where $\nu_\parallel \equiv 2\nu_\perp \equiv 2\nu'$. In equation (1), ν' and z' denote the critical exponents of the transverse correlation length and the relaxation time of the transverse fluctuations of the flux lines, respectively. In the limit of small current, one expect that, above T_{BG}, the scaling function $F_+(x \to 0) \to$ constant, leading to an ohmic resistivity, as expected just above T_{BG} in the thermally dominated vortex liquid. Below T_{BG}, $F_-(x \to 0) \approx \exp(x^{-\mu})$, which describes the glassy behaviour of the system. Finally approaching the transition, $F_\pm(x) \approx x^{(z'-2)/3}$ as $x \to \infty$ with the result that $\rho \approx J^{(z'-2)/3}$ remains finite at $T = T_{BG}$. At $T = T_{BG}$, the $I(V)$ curves are expected to show a power law dependence $V \approx I^{(z'+1)/3}$. In $F_\pm(x)$, J is scaled by $J_x = k_B T/(\ell_\parallel \ell_\perp \Phi_0)$ in such a way that the thermal effects dominate the current effects as $J < J_x$. Generally, the estimated values of the dynamic exponent z' and the static exponent ν' can be obtained from the ohmic resistance (linear part of I–V curves in the limit $I \to 0$) in the thermally assisted flux-flow regime which should vanish according to $R \approx [(T - T_{BG})/T_{BG}]^{\nu'(z'-2)}$. In this basis, a plot of $(\mathrm{d} \ln R/\mathrm{d}T)^{-1} = (T - T_{BG})/[\nu'(z' - 2)]$ versus temperature should be a straight line with a slope equal to $1/[\nu'(z' - 2)]$ intercepting the abscissa axis at T_{BG}. As shown in figure 3, plots of $[(\mathrm{d} \ln R/\mathrm{d}T)]^{-1}$ versus T are consistent with this type of behaviour. We obtain therefrom $[\nu'(z' - 2)] \approx 4$ and $T_{BG} = 72.4$ and 71 K, for $B = 0.2$ and 0.5 T, respectively. A second way to determine the BG temperature and the critical exponents is from scaling laws of the I–V characteristics. Figures 2 and 4 display a fit of equation (1) to the data obtained in sample 1 over a wide range of filling fractions $0.133 \leqslant f = B/B_\Phi \leqslant 0.8$. From scaling analysis, the optimum values of the critical exponents $z' = 5.27 \pm 0.05$ and $\nu' = 1.3 \pm 0.07$ are extracted and found to be field independent. In table 1, we summarize the critical exponents z' and ν' estimated from the scaling analysis at each magnetic field in all samples. These values agree reasonably with simulations predictions $z' = 6 \pm 0.5$ and $\nu' = 1 \pm 0.01$ [25] and other experimental results on

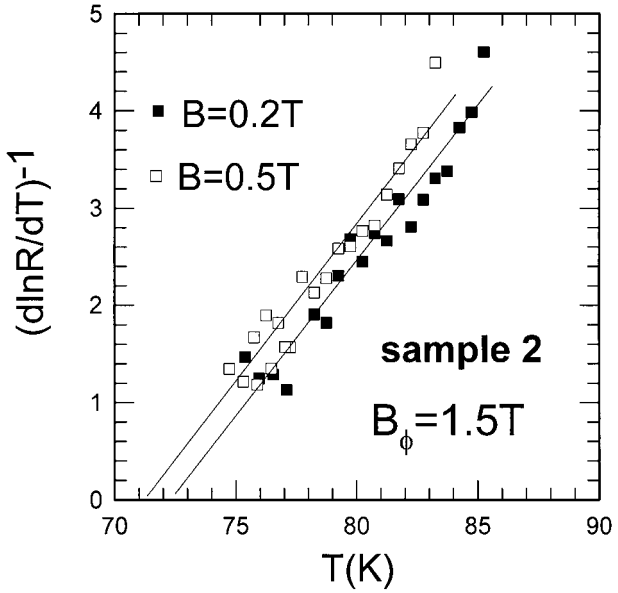

Figure 3. Typical inverse of the logarithmic derivative of the resistance $R(T)$ for $B = 0.2$ and 0.5 T. The solid lines represent a fit to the power law $R \approx (T - T_{BG})^{\nu'(z'-2)}$, with a slope $[\nu'(z'-2)]^{-1} \approx 0.26$ and intercept $T_{BG} = 72.4$ and 71 K, respectively.

$Tl_2Ba_2CaCu_2O_8$ thin films [26, 27]. Whereas there is a large scattering in reported exponents values $z' \approx 2.2$–8.8 and $\nu' \approx 0.9$–1.6 on YBCO single crystals and thin films, respectively [28–31]. In BSCCO, a combined critical exponent value $n = \nu'(z'-2) \approx 9$ and 8.5 is extracted from the in-plane and out-of-plane resistivity data, respectively [32, 33]. This value is twice that found in our study. From asymptotic behaviours of scaling functions F_+ and F_-, shown in figure 4 (horizontal $F_+ = 1$ and oblique $F_+ = x^{(z'-2)/3}$ solid lines), we have extracted two quantities R_0 and I_x, which can be related to samples normal resistivity and vortex-loop area, respectively. The vertical dashed line gives an estimate for the current crossover separating the ohmic and non-ohmic behaviour $J_{0x} - k_B T(\ell_{0\|}\ell_{0\perp}\Phi_0)$ for $T < T_{BG}$. We use J_{0x} as the way to reach the quantity $(\ell_{0\|}\ell_{0\perp})^{1/2} \approx 20$–$30$ Å. Figure 5, whose axes are normalized by R_0 and I_x, shows that all data obtained in three samples collapse on two filling factor independent curves F_+ and F_-. We emphasize two remarkable points. First, we find that for all samples, z' and ν' are independent of filling factors as shown in the inset of figure 5. Second, the critical exponents z' and ν' appear to be, within the experimental errors, sample and dose irradiation independent. The absence of field, sample and dose irradiation in the exponents z' and ν' provides a demonstration of a universal behaviour as expected in the Bose-glass transition [4]. The only field dependent fitting parameter in figure 5 is T_{BG}, in such a way that $T_{BG}(B)$ defines the BG line transition in the B–T phase diagram.

We now investigate the BG phase itself ($T < T_{BG}$). The dominant mechanism for low energy excitations is assumed to be vortex superkinks between line defects. In the low current density limit, the relevant excitations can be described by a variable-range-hopping (VRH) behaviour with a strongly nonlinear expression

$$E = \rho_0 J \exp\lfloor -E_K/k_B T(J_0/J)^{\mu}\rfloor \tag{2}$$

where ρ_0 is a characteristic flux-flow resistivity, E_K is the typical kink energy, J_0 is the characteristic current scale. The value of the glass exponent μ is typical of vortex-

Table 1. Measured critical exponents $z'(\pm 0.05)$ and $\nu'(\pm 0.07)$ as a function of filling factor for all samples.

	Sample 1		Sample 2		Sample 3	
	z'	ν'	z'	ν'	z'	ν'
0.067	5.3	1.2	—	—	—	—
0.133	5.28	1.195	5.25	1.28	5.34	1.37
0.2	5.2	1.23	—	—	—	—
0.267	5.3	1.3	5.26	1.28	5.34	1.36
0.333	—	—	—	—	—	—
0.4	—	—	5.24	1.35	5.37	1.37
0.467	5.23	1.22	—	—	—	—
0.533	—	—	5.25	1.35	5.3	1.3
0.567	5.24	1.25	5.30	1.3	—	—
0.667	5.3	1.3	5.16	1.38	5.21	1.32
0.8	—	—	5.3	1.3	5.3	1.4
0.9	5.29	1.36	—	—	—	—

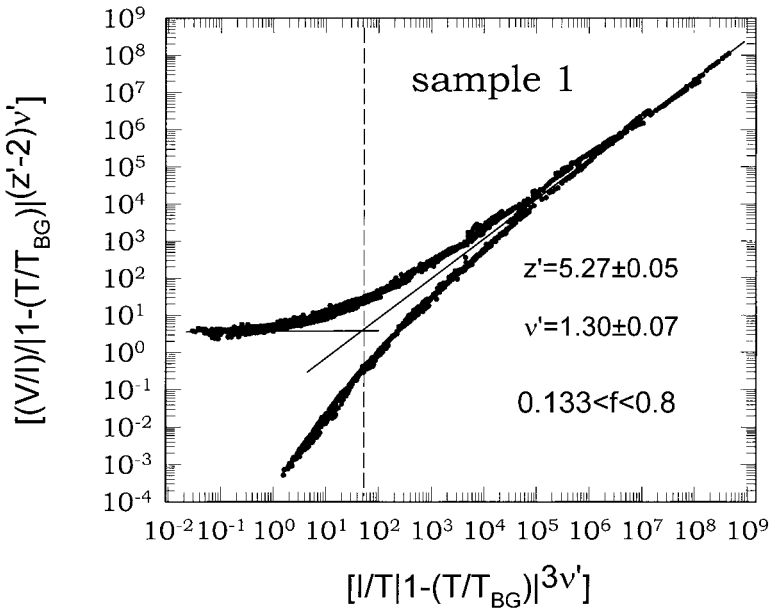

Figure 4. Scaling law I–V curves obtained at filling fractions $0.026 \leqslant f \leqslant 0.9$ in sample 3 with $f = 0.1$, 0.133, 0.267, 0.4, 0.67, 0.8 and 0.9. The same scaling exponents $z' = 5.27 \pm 0.05$ and $\nu' = 1.30 \pm 0.07$ are used for all fields. According to equation (1), the upper and lower branches display Bose-glass universal functions F_+ and F_-, respectively.

loop excitations $\mu = 1$ and $\mu = 1/3$ for half loop and double-superkinks, respectively [4]. We extract the value of the VRH exponent μ by recasting equation (2) into the form $\mathrm{d}[\ln(E/J)]/\mathrm{d}J = (\mu E_K/J_0 k_B T)(J_0/J)^{\mu+1}$ so that a log–log plot of the graph of $\mathrm{d}[\ln(E/J)]/\mathrm{d}J$ versus J is a straight line, whose slope is equal to $-(\mu+1)$. Figure 6 displays log–log plots of $\mathrm{d}[\ln(V/I)]/\mathrm{d}I$ versus I corresponding to typical isothermal I–V curves for $T < T_{BG}$ for all samples. Parallel straight lines support equation (2) with a magnetic field independent exponent value $\mu \approx 1/3$, which is in good agreement with the VRH mechanism

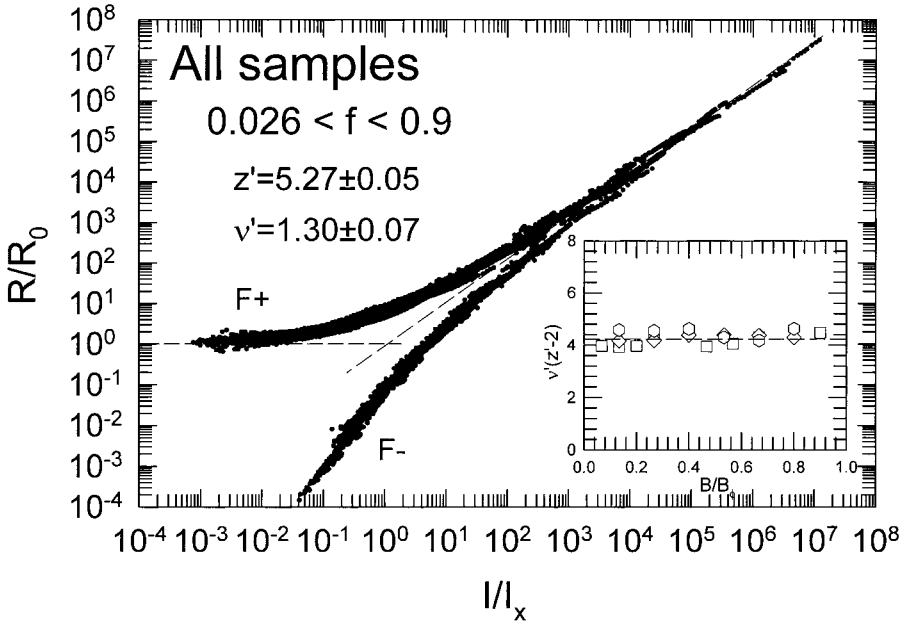

Figure 5. Universal scaling forms for the resistivity obtained in all samples over a wide range of filling factors $0.026 \leqslant f \leqslant 0.9$. The scaling obtained in figure 4 is normalized by R_0 and I_x. I_x is the current crossover separating the ohmic and non-ohmic regimes above T_{BG}. The inset shows the filling factor independent combined critical exponents $n = \nu'(z' - 2)$.

[34, 35]. A more extensive study has been performed in another paper, where the activation energy has been quantitatively estimated for the VRH in the same samples [36]. These experimental results, universal scaling of I–V characteristics and the VRH mechanism, provide support for the Bose-glass transition in our samples. This behaviour observed, at field below the matching field B_Φ, indicates that the vortices are correlated along the c-axis in BSCCO irradiated with heavy ions. This 3D coupling of vortices by CDs is clearly demonstrated by other experiments [33, 37, 38]. By contrast, for $B > B_\Phi$, we do not find any signature of VRH excitations characteristic of the BG phase at low temperatures. Figure 7 exhibits a typical log–log plot of isothermal I–V curves in this range of fields for samples 2 and 3. Now, there is no way to fit equation (1) to the data obtained in this regime. This indicates that vortex dynamics deviates from that of a Bose-glass. The dashed line in figure 7 displays the characteristic temperature $T_{crit}(B)$ determined by using a low ohmic resistance criterion $R_{crit} \approx 1\ \mu\Omega$ (R_{crit} determined from the linear part of I–V curves in the limit $I \to 0$). $T_{crit}(B)$ is the temperature at which the ohmic resistance is expected to disappear. The deviations from the Bose-glass predictions at fields greater than B_Φ is due probably to the creep of vortex pancakes from interstitial vortices not trapped by CDs, as suggested previously in [37] and [39].

3.2. Bose-glass line

In the following, we will focus on the behaviour of the $T_{BG}(B)$ lines obtained from scaling analysis, as presented before. The experimental B–T phase diagram, including the Bose-glass melting lines of samples 1, 2 and 3 are presented in figure 8. Also displayed is the line of the unirradiated reference sample ($x = 0$), which was obtained from R–T curves measured at different fixed fields, using a low ohmic resistance criterion $R_{crit} \approx 1\ \mu\Omega$. The BG lines

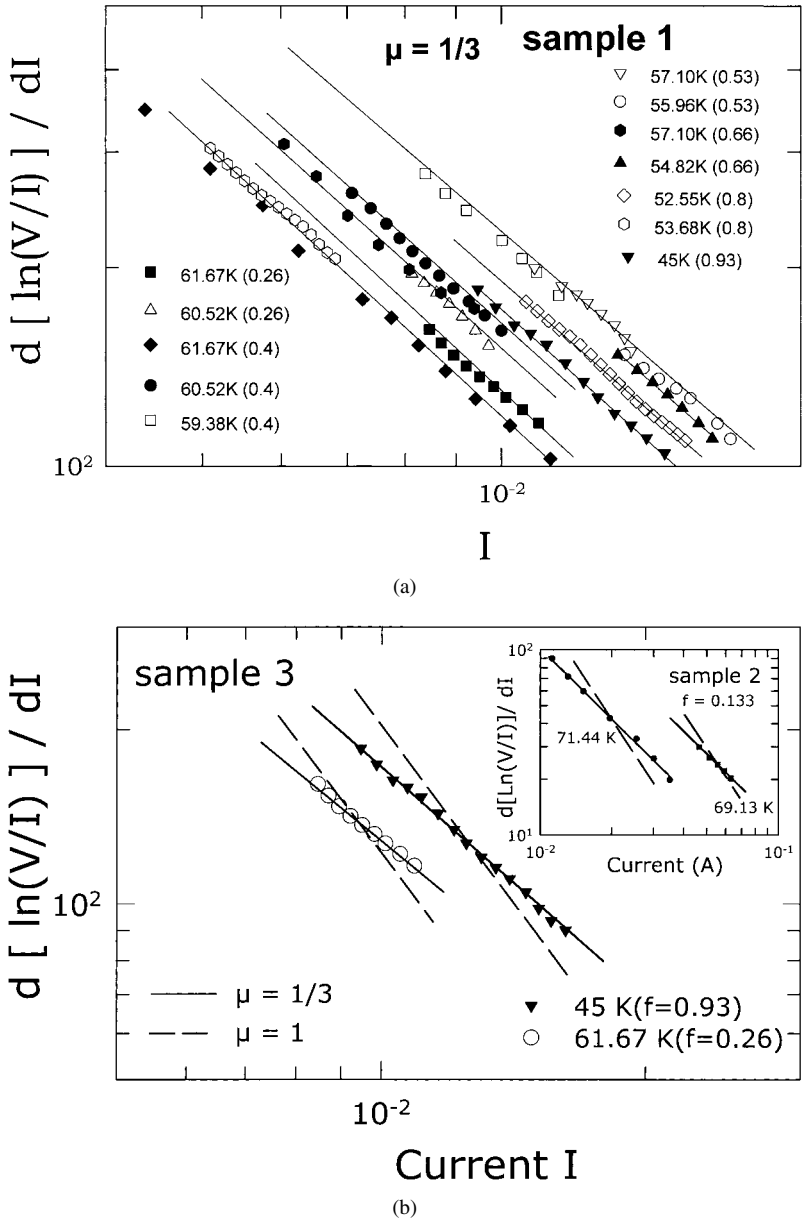

Figure 6. Log–log plot of $\mathrm{d}[\ln(V/I)]/\mathrm{d}I$ versus I for $T < T_{BG}$ obtained (a) on sample 1 and (b) samples 2 and 3. Parallel straight lines support equation (2) with $\mu \approx 1/3$, which is obtained for weak currents. As a comparison, the dashed lines represent an attempt to fit $\mathrm{d}[\ln(V/I)]/\mathrm{d}I \approx (I)^{-(\mu+1)}$ with $\mu = 1$ (figure 6(b)).

shown in figure 8 have similar features compared with those reported by Zech *et al* [40] and Doyle *et al* [41]. According to previous papers [42], we observe a pronounced shift of the $T_{BG}(B)$ lines for all irradiated samples to higher fields and temperatures due to the presence of columnar defects. Also, as may be seen in the figure the form of these lines exhibits some features which are not observed in the melting line of the pristine crystal. The first is the presence of a clear change (kinks) in the shape of $T_{BG}(B)$ lines, which occurs in the vicinity

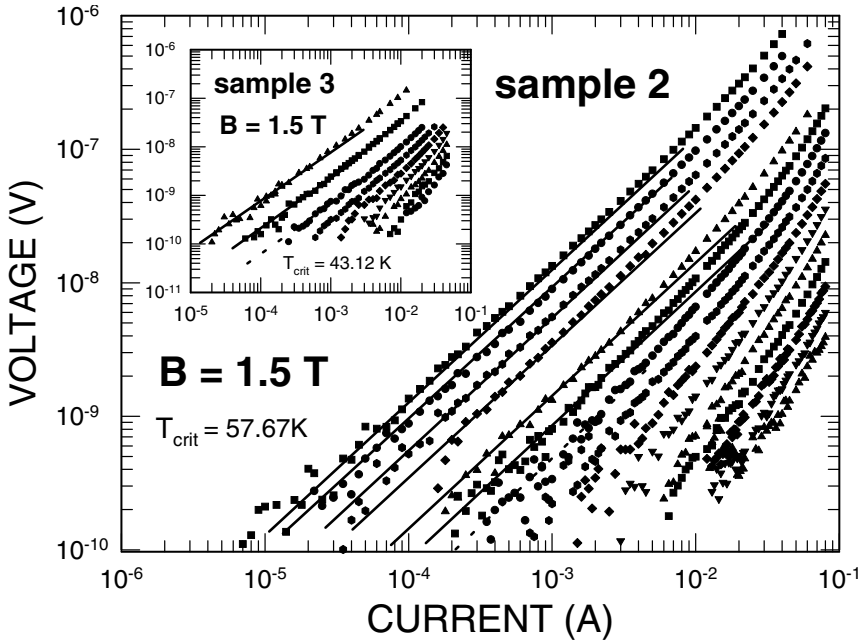

Figure 7. Typical isothermal I–V curves for $B \geqslant B_\Phi$. The dashed line displays the characteristic temperature determined with a low resistivity criterion $R_{crit} \approx 1\ \mu\Omega$. The straight lines display a fit of the Ohm law.

of characteristic fields $B \approx B_\Phi$ and $B \approx B_\Phi/3$, for all samples, as shown in figure 8. A similar first kink occurring near B_Φ was previously observed in YBCO single crystals [13] and thin films [30], irradiated parallel to the sample c-axis, at a crossover field $B_{cr} = 0.5B_\Phi$ and B_Φ, respectively. This crossover field separates a linear behaviour in (T_{BG}/T_c) above these values from a theoretically predicted curvature (equation (4) see text below). This change in the shape of the Bose-glass melting line (kink) near half the matching field was related to theoretical expectations [4] and experimental determination for $B^*(T)$ (from the drop of the persistent current density $J(T)$ at several fields, i.e. from the maximum in $-\mathrm{d}\ln J/\mathrm{d}T$) [10], and identified as a crossover from a region of strongly localized single-vortex pinning on CDs to a region of weak localization due to vortex–vortex interactions.

A theoretical detailed study of the $T_{BG}(B)$ behaviour was reported by NV [4] and Blatter *et al* [1] in the field region $B < B^*(T)$. They predict a power law for intermediate field $\Phi_0/\lambda_{ab}^2 < B \leqslant B_\Phi$ (i.e. $d_r \leqslant a_0 < \lambda_{ab}$) of the B–T phase diagram. In this range, the Bose-glass line $T_{BG}(B)$ is compared with the melting line $T_m(B)$ of the unirradiated material. In this regime, the Lindemann criterion which accounts for the contribution of correlated disorder described in [1] and [4], has been used for estimate of the shift of the melting line due to columnar disorder. In this approach, the derived Bose-glass temperature T_{BG} depends on the defect density as

$$T_{BG} = T_m[1 + (\pi^2 C_L a_0/2d)(T^*/T_m)^2] \tag{3}$$

with $d \approx \sqrt{\Phi_0/B_\Phi}$ the mean distance between columns, $T^* = \max(C_0, \sqrt{2})\sqrt{\tilde{\varepsilon}_1 U_0}$ is the energy scale for pinning disorder, $U_0 = (\varepsilon_0/2)\ln[1+(c_0/\sqrt{2}\xi_{ab})^2]$ is the mean pinning energy, $\tilde{\varepsilon} \approx \varepsilon\varepsilon_0 \ln(a_0/\xi_{ab})$ the tilt modulus where ε is the anisotropic parameter, $\varepsilon_0 = (\Phi_0^2/4\pi\mu_0\lambda^2)$ is the line tension and $a_0 \approx \sqrt{\Phi_0/B}$ is the vortex-lattice constant. Equation (3) can be rewritten

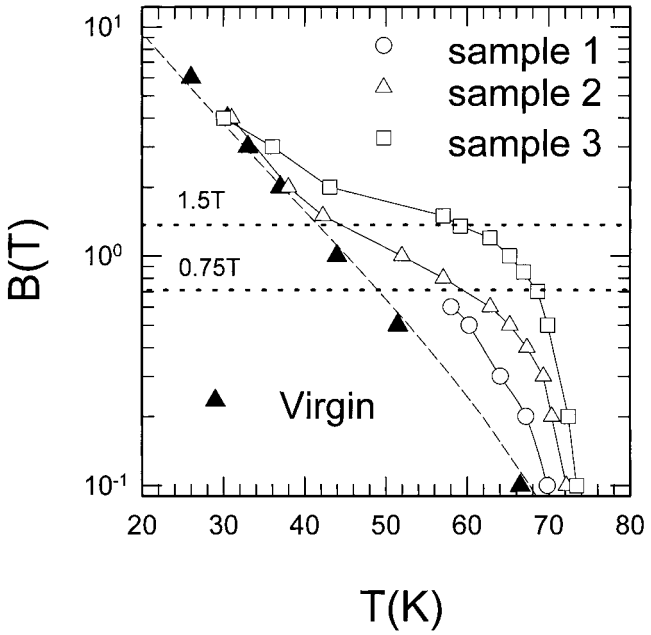

Figure 8. Bose-glass $T_{BG}(B)$ lines for irradiated sample 1 ($B_\Phi = 1.5$ T) and 2 ($B_\Phi = 0.75$ T). Solid lines are guides to the eye. Filled triangles: melting line of the pristine sample $Bi_2Sr_2CaCu_2O_8$, using an $R_{crit} = 10\ \mu\Omega$ criterion.

in a simple form containing only a single parameter Γ describing the effect of disorder [1]

$$T_{BG}(B) \approx \Gamma T_m(B) + (1-\Gamma)T_c\left[1 - \frac{2\pi B\xi_{ab}^2(0)}{\Phi_0}\right] \tag{4}$$

where $\Gamma = [1 + (1/16C_L\sqrt{G_i})C_0^2/\xi(0)d]^{-1}$ is the disorder related parameter that contains both thermal $(G_i)^{1/2}$ and irradiation-induced $[C_0^2/\mathrm{d}\xi(0)]$ fluctuations. The first-order melting $T_m(B)$ line, obtained by the conventional Lindemann criterion in a sample without columnar defects, can be written as [1]

$$T_m(B) = \left(\frac{\alpha T_c}{\alpha + T_c}\right)\left(1 - \frac{2\pi B\xi_{ab}^2(0)}{\Phi_0}\right) \tag{5}$$

with $\alpha = (C_L a_0 T_c/\xi_{ab}\sqrt{G_i})$ where $a_0 \approx \sqrt{(\Phi_0/B)}$ is the vortex spacing. The Lindemann number C_L is usually chosen to be a constant of order $C_L \approx 0.1$–0.3. Here G_i is the Ginzburg number, which is given for a 3D anisotropic oxide superconductor by [1]

$$G_i = \left(\frac{2\pi\mu_0 k_B T_c \lambda_{ab}^2(0)\gamma}{\Phi_0^2\xi_{ab}(0)\sqrt{2}}\right)^2 \tag{6}$$

where γ denotes the mass anisotropy ratio.

Further, we have attempted to fit equation (4) to our experimental results. The solid lines shown in figure 9 represent the theoretical $T_{BG}(B)$ lines normalized by the matching field against the normalized temperature, using the diameter of defects C_0 as the only fitting parameter. The average values of the other fitting parameters, shown in figure 9 are: $\xi_{ab} = 18$ Å [19], $\lambda_{ab} = 1850$ Å [19] (these values are determined from magnetization measurements conducted on the same samples), $\gamma = 50$ [1] and a reasonable Lindemann value $C_L \approx 0.28$.

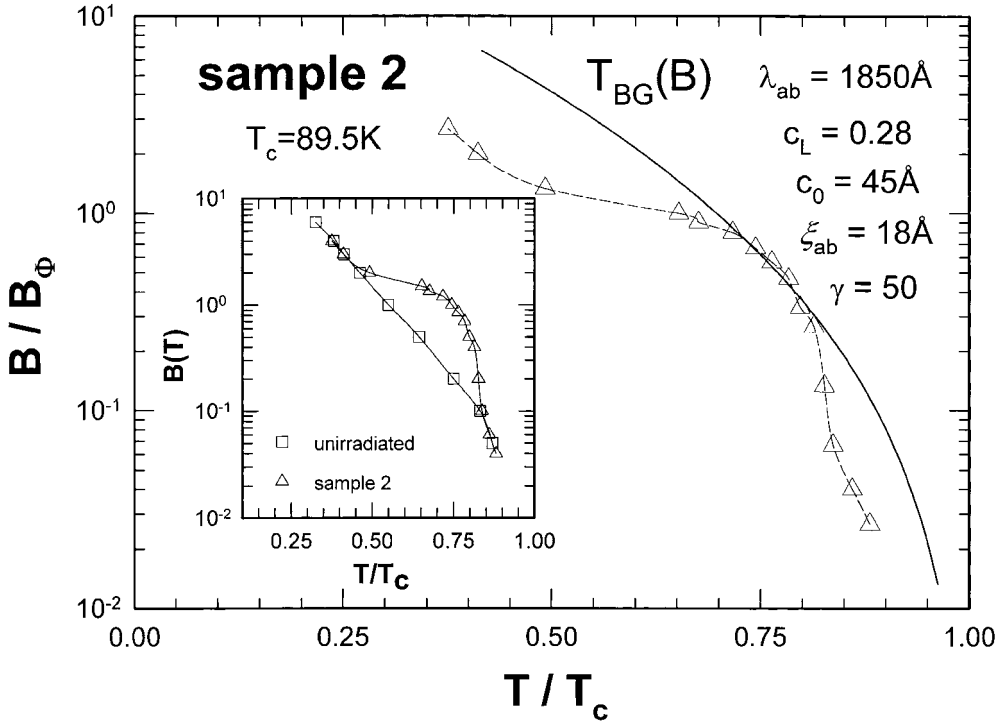

Figure 9. Magnetic-field dependence of the transition temperature resulting from scaling analysis for sample 2. The solid line represents the fit from equation (4) to the data. The inset shows the data determined by using an ohmic resistivity criterion in the unirradiated reference sample and irradiated sample 2.

Figure 8 leads to two main features. First, the theoretical curves and experimental data quantitatively agree over a magnetic field range $0.3B_\Phi < B < 0.8B_\Phi$, with a defect diameter $2C_0 \approx 90$ Å, which is typical for damage tracks produced with 5.8 GeV Pb-ion beams in such compounds [43]. Second, it should be noted that beyond this interval, in high field (i.e. low temperature) and high temperature (i.e. low field) regimes, the fit fails and the lines converge to the line measured in the pristine sample by the low resistivity criterion. This clearly demonstrates that the influence of the columnar defects changes with the filling fraction $f = (B/B_\Phi)$ and the level of thermal fluctuations.

3.3. Vortex phase diagram

Our experimental BG lines obtained in three irradiated samples are summarized in figure 10. A similar vortex phase diagram has recently been derived from numerical simulations using the Monte Carlo method [44]. Figure 10 shows strong evidence for the existence of the temperature interval [$T = 0.72\ T_c$, $T = 0.83\ T_c$], where the BG melting lines for three irradiated samples can be scaled on top of each other. Further, it implies that in this temperature range the vortex interactions with CDs is not sensitive to doses of irradiation and sample. On the other hand, in this regime the BG melting line follows the accommodation field B^* which separates the strongly localized regime from the weak pinning regime, as can be seen in figure 10. According to the NV theory [4], $B^* \approx (C_0/2\xi_{ab})^2(1-(T/T_c))$ decreases linearly above the temperature T_0 up to the depinning temperature T_1. This result suggests that the maximum effect of CDs is

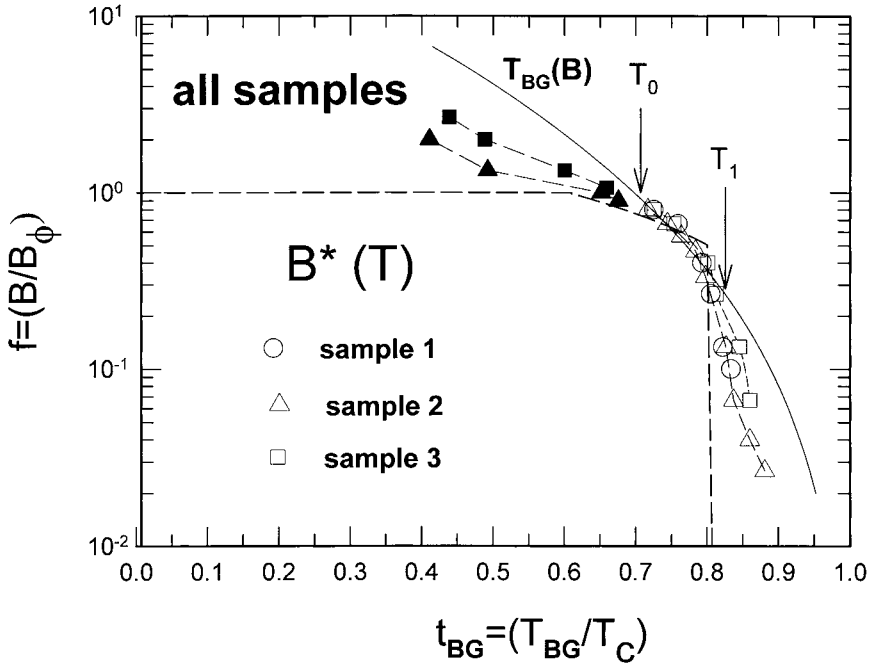

Figure 10. Schematic magnetic phase diagram of the $Bi_2Sr_2Ca_{1-x}Y_xCu_2O_8$ compound over a wide range of filling fractions f (open symbols). The line $B^*(T)$ denotes the boundary in the Bose-glass phase which separates a single-vortex strong and a weaker collective pinning regime [1, 4]. The solid line is a fit of the theoretical expression $T_{BG}(B)$ (equation (4)) to the data extracted from scaling analysis in the samples 1, 2 and 3, respectively. The best fit of $T_{BG}(B)$ from equation (4) to data between $t_0 = (T_0/T_c) \approx 0.72$ and $t_1 = (T_1/T_c) \approx 0.83$ is obtained with defect diameters $2C_0 \approx 90$ Å. The filled symbols represent the data determined by using a low ohmic resistivity criterion $R_{crit} \approx 1\ \mu\Omega$ ($f > 1$, i.e. $B > B_\Phi$).

expected around $B \approx 0.8\ B_\Phi$. Our observations in the low temperature (i.e. high field) regime ($T < 0.72\ T_c$ and $B > 0.8\ B_\Phi$) are in agreement with previous studies [1, 4, 12], showing that the vortex system is dominated by the vortex–vortex interactions. For $T > 0.83\ T_c$, the $T_{BG}(B)$ line coincides with $T_m(B)$ according to the view that disorder effects should be negligible at low field and high temperature for which the pinning by disorder is smoothed by the thermal fluctuations. Such behaviour is experimentally found in highly anisotropic compounds in the presence of point disorder [45–47] and BSCCO single crystals with columnar defects [6, 14, 43]. Finally, it is interesting to point out that in the temperature range [$T = 0.72\ T_c$, $T = 0.83\ T_c$], the enhancements of pinning after irradiation are the same at the same reduced temperature and filling factor. This shows the universality of our observations for each sample. Such behaviour is in good agreement with those obtained in melt-textured $YBa_2Cu_3O_{7-\delta}$ [48] and $Bi_2Sr_2CaCu_2O_8$ single crystals [33, 49].

The kinks observed around $0.3\ B_\Phi$ and B_Φ in the Bose-glass melting lines can be related to two characteristic temperatures T_0 and T_1 in [1] and [4], respectively. Indeed, as pointed out by Zech *et al* [6], the first temperature $T \approx 0.72\ T_c$ was identified with the crossover temperature T_0 separating the low and high temperature limits defined by the relation $C_0\sqrt{2}\xi_{ab}(T_0)$. Using $\xi_{ab} = 18$ Å and $C_0 = 45$ Å, we find $T_0 = [1 - 2(\xi_{ab}/C_0)^2]T_c \approx 0.68\ T_c$. The second temperature $T \approx 0.83\ T_c$ was related by many authors [40, 43, 50] to the depinning temperature, i.e. the temperature at which the thermal energy becomes comparable to the pinning energy. This experimental value $T \approx 0.83\ T_c$ is in good agreement with the previous

experimental determinations which were derived from magnetic measurements $T_1 \approx 0.85\ T_c$ [40] and $T_1 \approx 0.83\ T_c$ [43, 50]. The theoretical value (equation (D7) of [4]) indicates that

$$\frac{T_1}{T_c} = \frac{(C_0/4\xi_{ab})\sqrt{(\ln \kappa / G_i)}}{1 + (C_0/4\xi_{ab})\sqrt{(\ln \kappa / G_i)}} \tag{7}$$

where G_i is the Ginzburg number given by equation (6) for the case of the anisotropic oxide superconductors. Using typical parameters, $C_0 = 45$ Å, $\xi_{ab} = 18$ Å, $\lambda_{ab} = 1850$ Å (sample 2) and $\gamma = 50$ we find that $T_1 \approx 0.46\ T_c$. This low value can be explained by the large value of G_i calculated from equation (6). This Ginzburg number value is many orders of magnitude larger than $G_i = 0.1$ [4], which is generally used for the theoretical estimates of the depinning temperature T_1 in the case of a highly anisotropic material such as Bi-2212. Nevertheless in some experiments using magnetic or transport measurements, T_1 has been found to be considerably higher ($T_1 \approx 0.83\ T_c$) [40, 43, 50]. For the highly anisotropic BSCCO, the 2D depinning temperature was estimated by Zech *et al* [40] to be $T_1 \approx d\alpha\varepsilon_0$, where d is the Cu layer spacing and $\alpha < 1$ is the pinning efficiency of columnar defects. Using a typical value of $d = 15$ Å [1] and our experimental value $T_1 = 0.81\ T_c$, one obtains $\alpha = 0.7$, which is in good agreement with other experimental results. Finally, the presence of a change (kink) in the vortex dynamics, which occurs in the vicinity of characteristic field $B \approx B_\Phi/3$ was also reported and discussed previously [15, 16, 51, 52]. These experiments show that this anomaly is associated with the recoupling of vortices at this characteristic field below the matching field B_Φ. Further investigations are necessary to clarify the influence of recoupling of vortices on the Bose-glass transition in this field regime.

4. Summary

I–V characteristics over a wide range of filling fraction $f = (B/B_\Phi)$ are used to investigate vortex dynamics in heavily-irradiated $Bi_2Sr_2CaCu_2O_8$ single crystals. We find experimental support for a Bose-glass transition at $T_{BG}(B)$ for magnetic field less than B_Φ aligned with columnar defects. Field and sample independent critical exponent values $z' = 5.27 \pm 0.05$ and $\nu' = 1.3 \pm 0.07$ have been found. This result is in good agreement with the well established universality rules for the critical exponents at a standard second-order transition. Our experimental phase diagram, extracted from scaling analysis, reveals various vortex pinning regimes that strongly depend on f. The obtained results show evidence that columnar defects control the dynamics of the vortex system (defect–vortex interactions, strong pinning) only between two characteristic temperatures $T_0 \approx 0.72\ T_c$ ($f \approx 0.8$) and $T_1 \approx 0.83\ T_c$ ($f \approx 1/3$). In this range, the Lindemann criterion which accounts for the contribution of correlated disorder seems well adapted to describe the BG melting line of such superconducting compounds. Moreover, beyond this interval, the vortex system is increasingly dominated by the vortex–vortex interactions (high field regime) or thermal fluctuations (high temperature regime). In these domains, the pinning by CDs is ineffective and the melting line approaches that for the defect free case.

References

[1] For a review, see Blatter G, Feigel'man M V, Geshkenbein V B, Larkin V B and Vinokur V M 1994 *Rev. Mod. Phys.* **66** 1125

[2] Giamarchi T and Le Doussal P 1997 *Phys. Rev.* B **55** 6577

[3] Fisher D S, Fisher M P A and Huse D A 1991 *Phys. Rev.* B **43** 130

[4] Nelson D R and Vinokur V M 1993 *Phys. Rev.* B **48** 13 060

[5] Nelson D R 1996 *Physica* C **263** 12

[6] Zech D, Lee S L, Keller H, Blatter G, Kes P H and Li T W 1996 *Phys. Rev.* B **54** 6129

[7] Konczykowski M, Chikumoto N, Vinokur V M and Feigel'man M V 1995 *Phys. Rev.* B **51** 3957

[8] Samoilov A V, Feigel'man M V, Konczykowski M and Holtzberg F 1996 *Phys. Rev. Lett.* **76** 2798
[9] Warmont F, Hardy V, Goupil Ch, Simon Ch, Provost J and Ruyter A 1997 *Physica* C **277** 61
[10] Krusin-Elbaum L, Civale L, Thompson J R and Feild C 1996 *Phys. Rev.* B **53** 11 744
[11] Cho J H, Safar H, Maley M P, Willis J O and Gray K E 1998 *Physica* C **302** 113
[12] Larkin A I and Vinokur V M 1995 *Phys. Rev. Lett.* **75** 4666
[13] Krusin-Elbaum L, Civale L, Blatter G, Marwick A D, Holtzberg F and Feild C 1994 *Phys. Rev. Lett.* **72** 1914
[14] Mezzetti E, Gerbaldo R, Ghigo G and Gozzelino L 1999 *Phys. Rev.* B **59** 3890
[15] Sato M, Shibauchi T, Ooi S, Tamegai T and Konczykowski M 1997 *Phys. Rev. Lett.* **79** 3759
[16] Chikumoto N, Kosugi M, Matsuda Y, Konczykowski M and Kishio K 1998 *Phys. Rev.* B **57** 14 507
[17] Radzihovsky L 1995 *Phys. Rev. Lett.* **74** 4923
[18] Wengel C and Tauber U C 1998 *Phys. Rev.* B **58** 6565
[19] Villard G, Pelloquin D and Maignan A 1998 *Phys. Rev.* B **58** 15 231
[20] Wahl A, Thopart D, Villard G, Maignan A, Simon Ch, Soret J C, Ammor L and Ruyter A 1999 *Phys. Rev.* B **60** 12 495
[21] Shimoyama J, Nakayama Y, Kitazawa K, Kishio K, Hiroi Z, Chong I and Takano M 1997 *Physica* C **281** 69
[22] Ruyter A, Simon Ch, Hardy V, Hervieu M and Maignan A 1994 *Physica* C **225** 235
[23] Villard G, Pelloquin D, Maignan A and Wahl A 1997 *Physica* C **278** 11
[24] Herbert S, Hardy V, Villard G, Hervieu M, Simon Ch and Provost J 1998 *Phys. Rev.* B **57** 649
[25] Wallin M and Girvin S M 1993 *Phys. Rev.* B **47** 14 642
[26] Ta Phuoc V, Ruyter A, Ammor L, Wahl A and Soret J C 1997 *Phys. Rev.* B **56** 122
[27] Budhani R C, Holstein W L and Suenaga M 1994 *Phys. Rev. Lett.* **72** 566
[28] Jiang W, Yeh N C, Reed D S, Kriplani U, Bean D A, Konczykowski M, Tombrello T A and Holtzberg F 1994 *Phys. Rev. Lett.* **72** 550
[29] Gammel P L, Schneemeyer L F and Bishop D J 1991 *Phys. Rev. Lett.* **66** 953
[30] Mazilu A, Saffar H, Maley M P, Coulter J Y, Bulaevskii L N and Foltyn S 1998 *Phys. Rev.* B **58** R8909
[31] Nakielski G, Rickertsen A, Steinborn T, Wiesner J, Wirth G, Jansen A G M and Kotzler J 1996 *Phys. Rev. Lett.* **76** 2567
[32] Mui L, Wagner P, Hadish A, Hilmer F and Adrian H 1995 *Phys. Rev.* B **51** 3953
[33] Seow W S, Doyle R A and Campbell A M 1996 *Phys. Rev.* B **53** 14 611
[34] Thompson J R, Krusin-Elbaum L, Civale L, Blatter G and Feild C 1997 *Phys. Rev. Lett.* **78** 3181
[35] Konczykowski M, Chikumoto N, Vinokur V M and Feigel'man M V 1995 *Phys. Rev.* B **51** 3957
[36] Soret J C, Ammor L, Ta Phuoc V, De Sousa R, Ruyter A, Wahl A and Villard G 1999 *Solid State Commun.* **109** 461
Soret J C, Ta Phuoc V, Ammor L, Ruyter A, De Sousa R, Olive E, Wahl A, Villard G and Simon Ch 2000 *Phys. Rev.* B **61** at press
[37] Kuroda N, Ishikawa N, Chimi Y, Iwase A, Okayasu S, Ikeda H, Yoshizaki R and Kambara T 1999 *Physica* C **321** 143
[38] Hanaguri T, Tsuchiya Y, Sakamoto S, Maeda A and Steel D G 1997 *Phys. Rev. Lett.* **78** 3177
[39] Van der Beek C J, Konczykowski M, Vinokur V M, Crabtree G W, Li T W and Kes P H 1995 *Phys. Rev.* B **51** 15 492
[40] Zech D, Lee S L, Keller H, Blatter G, Janossy B and Menovsky A A 1995 *Phys. Rev.* B **52** 6913
[41] Doyle R A, Seow W S, Yan Y, Campbell A M, Mochiku T, Kadowaki K and Wirth G 1996 *Phys. Rev. Lett.* **77** 1155
[42] Civale L, Marwick A D, Worthington T K, Kirk M A, Thompson J R, Krusin-Elbaum L, Sun Y, Clem J R and Holtzberg F 1991 *Phys. Rev. Lett.* **67** 648
[43] Herbert S, Hardy V, Villard G, Hervieu M, Simon Ch and Provost J 1998 *Physica* C **299** 259
[44] Sugano R, Onogi T, Hirata K and Tachiki M 1998 *Phys. Rev. Lett.* **80** 2925
[45] Ammor L, Soret J C, Smina A, Ta Phuoc V, Ruyter A, Wahl A, Martinie B, Lecomte J and Simon Ch 1997 *Solid State Commun.* **103** 393
[46] Mun M O, Lee S I, Cranfield P C, Cho B K and Johnston D C 1996 *Phys. Rev. Lett.* **76** 2790
[47] Khaykovich B, Zeldov E, Majer D, Li T W, Kes P H and Konczykowski M 1996 *Phys. Rev. Lett.* **76** 2555
[48] Mezzetti E, Gerbaldo R A, Ghigo G, Gozzelino L and Chrubini R 1997 *J. Appl. Phys.* **82** 6122
[49] Cho J H, Safar H, Maley M P, Willis J O, Couter J Y, Steel D J and Gray K E 1998 *Physica* C **302** 113
[50] Van der Beek C J, Konczykowski M, Vinokur V M, Li T W, Kes P H and Crabtree G W 1995 *Phys. Rev. Lett.* **74** 1214
[51] Yurgens A, Konczykowski M, Mros N, Winkler D and Cleason T 1999 *Phys. Rev.* B **60** 12 480
[52] Kosugi M, Matsuda Y, Gaifullin M, Bulaevskii N, Chikumoto N, Konczykowski M, Shimoyama J, Kishio K and Hirata K 1999 *Phys. Rev.* B **59** 8970